Electronic Supplementary Information

Colloidal properties and stability of colloidal activated carbon: Effects of aqueous chemistry on sedimentation kinetics

Ezinneifechukwunyelu U. Ndubueze, Hardiljeet K. Boparai, Laura Xu, Brent E. Sleep*

Department of Civil and Mineral Engineering, University of Toronto,
35 St. George Street, Toronto, ON, Canada M5S 1A4

Corresponding author email

*brent.sleep@utoronto.ca

S1. Characterization of Colloidal Activated Carbon (CAC)

1.1 Particle size distribution (PSD)

The size distribution of CAC was determined with dynamic light scattering (DLS) using a Horiba SZ-100 nanoparticle analyser in 2-openings polystyrene macro cuvettes (Brand®). The performance of the instrument was verified using Ludox® TM-50, at the beginning of all measurements. The appropriate concentration range for accurate measurements was first determined for the Ludox® TM-50 and then for the CAC. The selection criteria for appropriate concentrations were based on: (1) the concentration range at which the size distribution parameters were constant, (2) values correspond to expected values from literature, and (3) the shape and decay of autocorrelation curve was as expected for DLS measurements.

For Ludox® TM-50, the appropriate concentration range for accurate measurement of size distribution was selected as 0.16 - 2.5% at 25 ℃ (Fig. S1). The size range was 13-100 nm with a Z-average (D_z) of 32.93 ± 0.97 nm (Fig. S2), which is close to the previously reported size of 30-34 nm [1,2] and size range of 10-100 nm [2] by DLS. Similarly, the appropriate concentrations for determining size distribution of CAC were established as 0.0125 and 0.025% (Fig. S4 and S6).

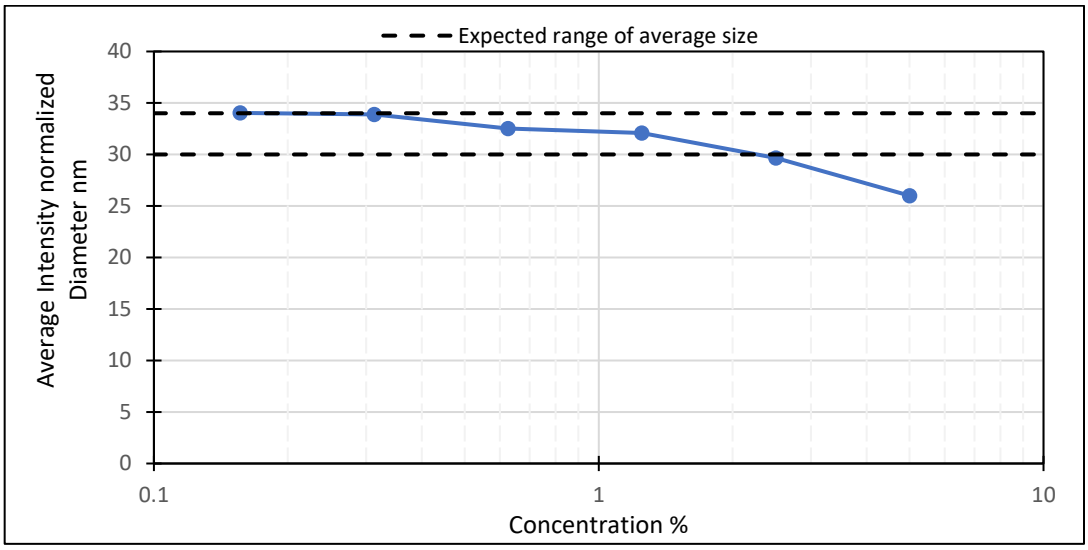

Fig. S1: Z-average of Ludox® TM-50 as a function of concentration.

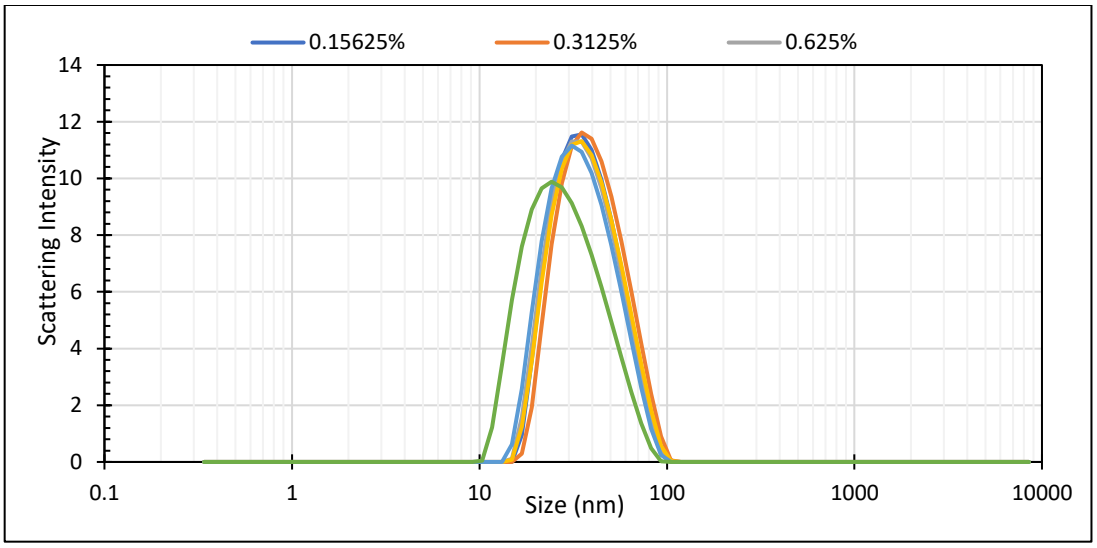

Fig. S2: Size distribution of Ludox® TM-50 at various concentrations.

Autocorrelation function decayed smoothly as expected for accurate dynamic light scattering (DLS) measurements at all concentrations selected (Fig. S3 for Ludox® TM-50 and Fig. S5 for CAC). Conditions, under which measurements were made, are summarized in Table S1 for Ludox® TM-50 and Table S2 for CAC.

Table S1 Experimental conditions used to determine the particle size of Ludox® TM-50.

Parameter	Value
Background electrolyte	MilliQ (material contains 0.135% m/m Na_2SO_4 [3])
Refractive index	1.45704 -0.000i
Temperature	25 ℃

Table S2: Experimental condition used to determine size of CAC.

Parameter	Value
Background electrolyte	Milli Q water
Refractive index	1.5-0.1i
Temperature	23 ℃

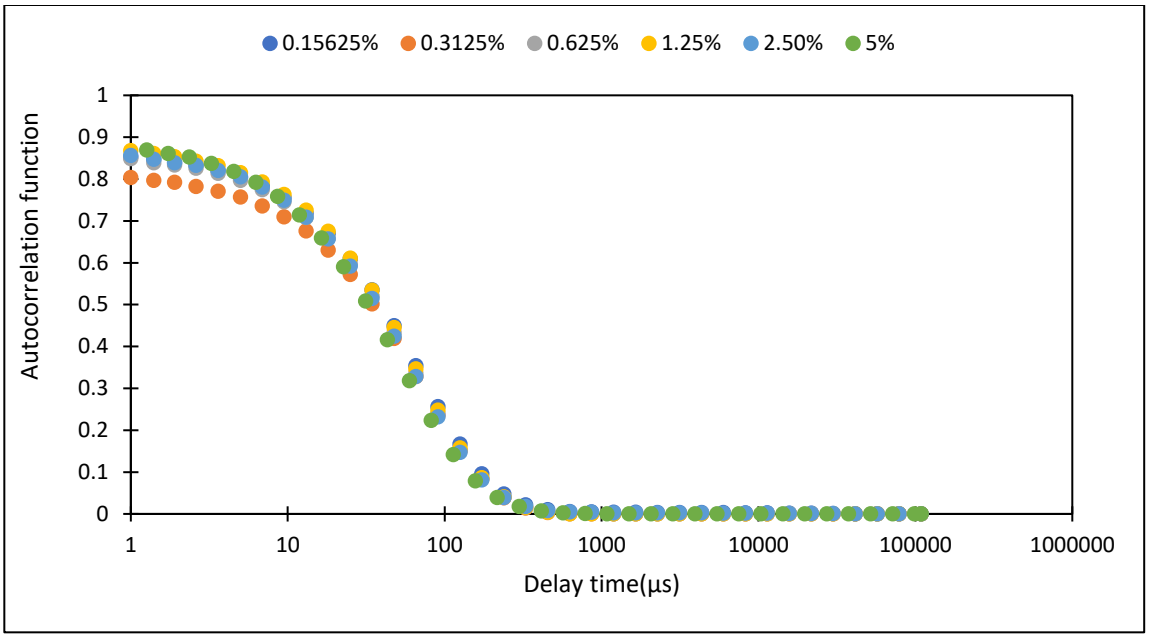

Fig. S3: Autocorrelation function for Ludox® TM-50 at varying concentrations.

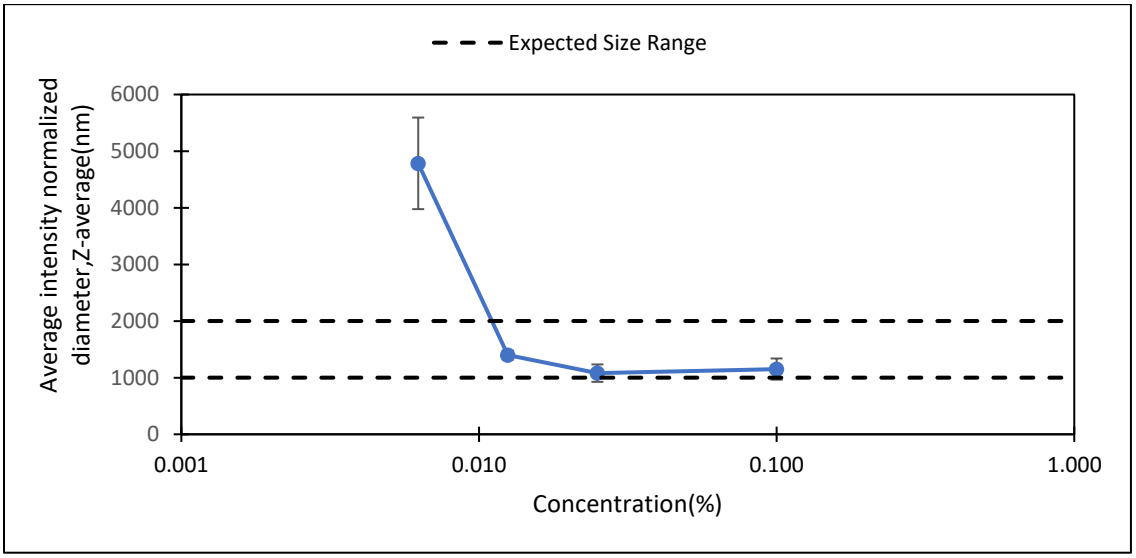

Fig. S4: Z-average of CAC as a function of concentration. Error bars represent standard deviation, n=5

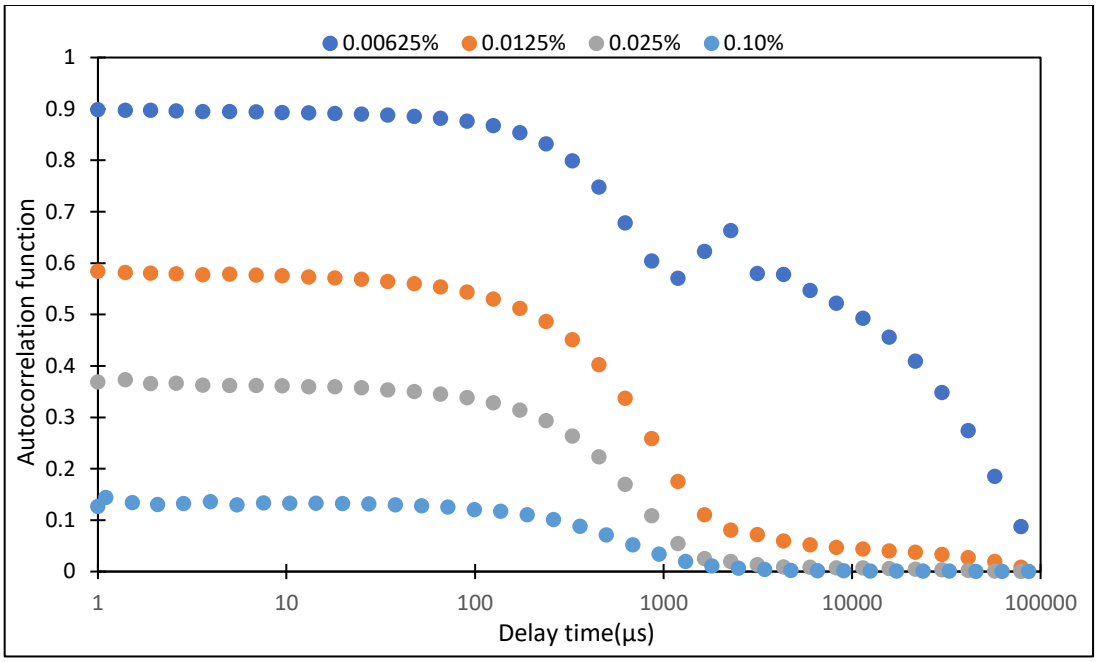

Fig. S5: Autocorrelation function for CAC at varying concentrations.

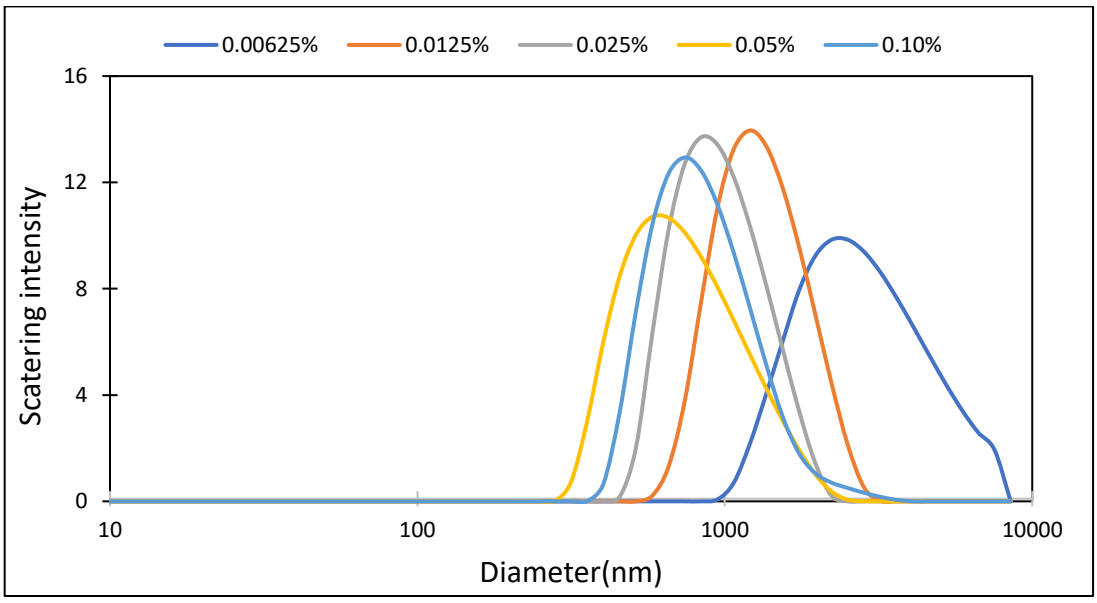

Fig. S6: Size distribution of CAC at various concentrations.

1.2 Electrophoretic mobility (EPM) and ζ-potential

ζ-potential was determined by measuring electrophoretic mobility (EPM) with DLS on the Horiba SZ-100 in carbon electrode zeta potential plastic cells. The performance of the instrument was verified using Ludox® TM-50. The EPM measurements were converted to ζ-potential by incorporating Helmholtz-Smoluchowski equation (κa >>1, ζ-potential ≤50mV) in the SZ-100 for Windows software version 1.90 (Horiba) and O'Brien & White (1978) equation (κa >>1, ζ-potential >50mV) in EXCEL (Microsoft Corporation). Appropriate concentration range for accurate ζ-potential measurements was first determined for Ludox® TM-50 and then for the CAC. The selection criteria for Ludox® TM-50 were same as the criteria 1 and 2 used for PSD (Section 1.1), with the exception that in this case constant and expected values of ζ-potential were used respectively. For the CAC, appropriate concentration range for accurate ζ-potential measurements was selected based on criteria 1 (constant value of ζ-potential) only.

The appropriate concentrations for accurate measurement of ζ-potential were determined as 10% and 15% for Ludox® TM-50 (Fig. S7) and 0.01 - 0.08% for CAC (see Fig. 1E). The ζ-potential of Ludox® TM-50 at 25 ℃ was found to be -37.3 ± 3.89 mV which is close to previously reported ζ-potential of -37 to -39 mV [1,2]. This value varied between 33-40 mV throughout the study. Conditions under which measurements were made a summarized in Table S3 for Ludox® TM-50 and Table S4 for CAC

Table S3: Experimental conditions used to determine ζ-potential of Ludox® TM-50. MilliQ was used since the electrolyte concentration in Ludox® TM-50 was enough for electrophoretic measurements. Additional electrolyte may lead to excessive aggregation and incorrect zeta potential.

Parameter	Value
Background electrolyte	MilliQ (however material contains 0.135% m/m Na_2SO_4 [3])
Temperature	25 ℃
Model on SZ-100 software	Smoluchowski

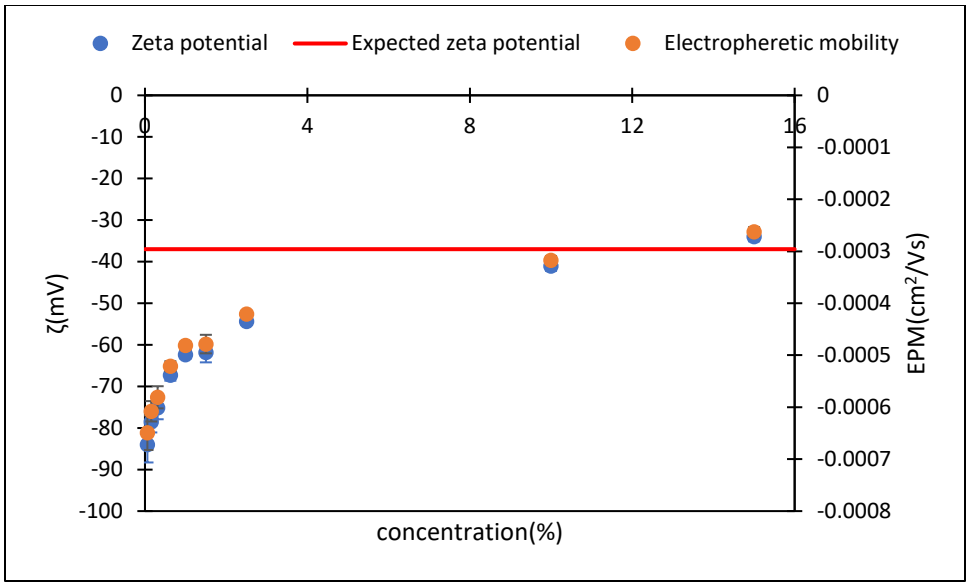

Fig. S7: ζ-potential and EPM of Ludox® TM-50 as a function of concentration. Error bars represent standard deviation, n=3.

Table S4: Experimental condition used to determine ζ-potential of CAC.

Parameter	**Value**
Background electrolyte	0.01M NaCl
Temperature	25 ℃
Model	Helmholtz-Smoluchowski (κa>>1, ζ-potential ≤50mV) O'Brien & White (1978) (κa>>1, ζ-potential >50mV)

S2. Measurement of PZC and IEP

2.1 Experimental conditions for PZC and IEP

The experimental conditions, under which PZC, IEP, and ζ-potential were measured, are summarized in the table below as recommended by Lowry *et al.* [5].

Table S5: Experimental conditions for determination of PZC and IEP of CAC.

Parameter	Value
Shaker type	Wrist action Shaker
Acid	0.1M HCL
Base	0.1M NaOH
Background electrolyte	0.001M to 0.1M NaCl
Material container	HDPE
Equilibration time	48 hrs
DLS Temperature	22.9 ± 0.09 ℃
CAC concentration	0.025%
PZC method	Batch titration [6]
EPM to ζ-potential model	Helmholtz-Smoluchowski (κa>>1, ζ-potential ≤50mV) O'Brien & White (1978) (κa>>1, ζ-potential >50mV)
Assumed shape	Spherical
Viscosity	$0.9*10^{-4}$-$1*10^{-4}$ Pa.m
Applied Voltage	1.4 ± 0.3 V (0.1M NaCl) 3.3 ± 0.0 V (0.01M, 0.001M NaCl)
Replicates	Samples=3, number of measurements =5
Conductivity	10.395 ± 0.235 mS/cm (0.1M NaCl) 0.865 ± 0.051 mS/cm (0.01M NaCl) 0.220 ± 0.054 mS/cm (0.001M NaCl)

S3. Experimental set up for stability of CAC under different types of cations and DOM.

Table S6: Experimental conditions used to determine effects of cations and DOM on ζ-potential of CAC.

Parameter	**Values**					
	Cations			**DOM**		
Shaker type	Wrist action Shaker					
pH	9	7	3	9	7	3
Acid	Milli Q only	0.1M HCl		Milli Q only	0.1M HCl	
Background electrolyte	0.001-0.3M Cl^- (0.0005-0.1M Ca^{2+}/Mg^{2+}, 0.001-0.3M K^+/Na^+)			0.001M NaCl		
Material of sample container	HDPE					
Equilibration time	48					
Temperature	22.9 ± 0.08 ℃					
CAC concentration	0.025%					
EPM to ζ-potential model	Helmholtz-Smoluchowski (κa>>1, ζ-potential ≤50mV) O'Brien & White (1978) (κa>>1, ζ-potential >50mV)		Helmholtz-Smoluchowski (κa>>1, ζ-potential ≤50mV)	Helmholtz-Smoluchowski (κa>>1, ζ-potential ≤50mV) O'Brien & White (1978) (κa>>1, ζ-potential >50mV)		Helmholtz-Smoluchowski (κa>>1, ζ-potential ≤50mV)
Assumed shape	Spherical					

Viscosity	$0.9*10^{-4}$ - $0.945*10^{-4}$ Pa.m			$0.9*10^{-4}$-$1*10^{-4}$ Pa.m		
Applied Voltage	3.4-1.3 V (0.0005-0.1M Ca^{2+}/Mg^{2+}) 3.4-0.8 V (0.001-0.3M K^{+}/ Na^{+})	3.4-1.3 V (0.0005-0.1M Ca^{2+}/Mg^{2+}) 3.3-0.8 V (0.001-0.3M K^{+}/ Na^{+})	3.3-1.2 V (0.0005-0.1M Ca^{2+}/Mg^{2+}) 3.3-0.8 V (0.001-0.3M K^{+}/Na^{+})	3.4 ± 0.12 V	3.4 ± 0.05 V	3.3 ± 0.00 V
Replicates	3					
Conductivity	0.17-19.281 mS/cm (0.0005-0.1M Ca^{2+}/Mg^{2+}) 0.182-35.057 mS/cm (0.001-0.3M K+/ Na+)	0.174 - 19.461 mS/cm (0.0005-0.1M Ca^{2+}/Mg^{2+}) 0.182-35.551 mS/cm (0.001-0.3M K+/ Na+)	0.371-19.129 mS/cm (0.0005-0.1M Ca^{2+}/Mg^{2+}) 0.452-35.404 mS/cm (0.001-0.3M K^{+}/ Na^{+})	0.143 ± 0.041 mS/cm (HA) 0.165 ± 0.005 mS/cm (BSA)	0.182 ± 0.063 mS/cm (HA) 0.176 ± 0.010 mS/cm (BSA)	0.313 ± 0.041 mS/cm (HA) 0.333 ± 0.024 mS/cm (BSA)

S4. Aggregation kinetics of 0.025% CAC by time-resolved DLS on Horiba SZ-100

During preliminary tests, the CAC (0.025%) showed no changes in size over 60 minutes of size measurements (Fig. S8), even though its particle settling behavior was noticeably different in 0.1M NaCl (0.1 Eq/L) versus 0.1M $CaCl_2$ (0.2 Eq/L) in the visual sedimentation experiments (Fig. S9) at 40 minutes. The inability of DLS to detect this visually observed difference can be attributed to the fundamental principle of DLS measurement, in which particle movement is solely governed by Brownian motion. No random movement of particles would happen if sedimentation occurs. In the absence of random particle motion, the number of particles in a constant volume of sample during measurements will vary over a short duration of time [11,12] and, thus, changes in size cannot be accurately determined. Because it is important to know how groundwater chemistry affects the stabilizing polymer of CAC, steps were taken to prevent its sedimentation during DLS measurement by filtering out large-sized particles of CAC which, in turn, would reduce its concentration.

The filtration protocol for CAC was as follows: the suspension (0.025% CAC) was first filtered with a 1 µm Whatman™ Grade GF/B glass microfiber filter paper (Cytvia) and then the filtrate was passed through a 0.45 µm, 47 mm Magna™ Nylon filter paper (Maine Manufacturing, LLC). The filtered suspension was kept at room temperature on a wrist-action shaker, to avoid particle settling prior to the start of aggregation kinetics experiment. The Z-average of filtered 0.025% CAC control (without NaCl or $CaCl_2$), obtained throughout the experiment, was 472.4 ± 35.5 nm.

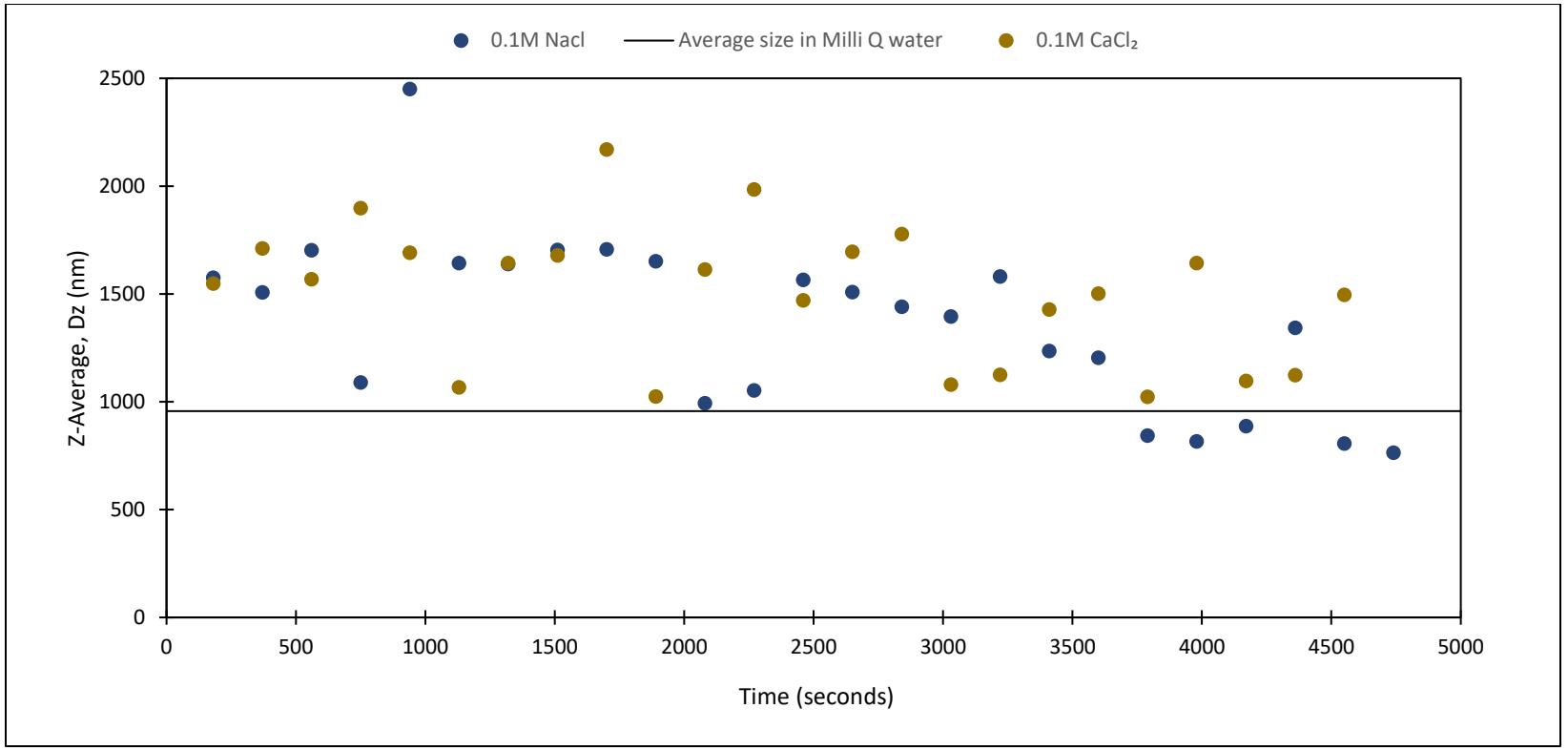

Fig. S8 Aggregation kinetics of 0.025% CAC in the presence of 0.1M NaCl (0.1 Eq/L), Milli-Q water, and 0.1M $CaCl_2$ (0.2 Eq/L) at pH = ~8.

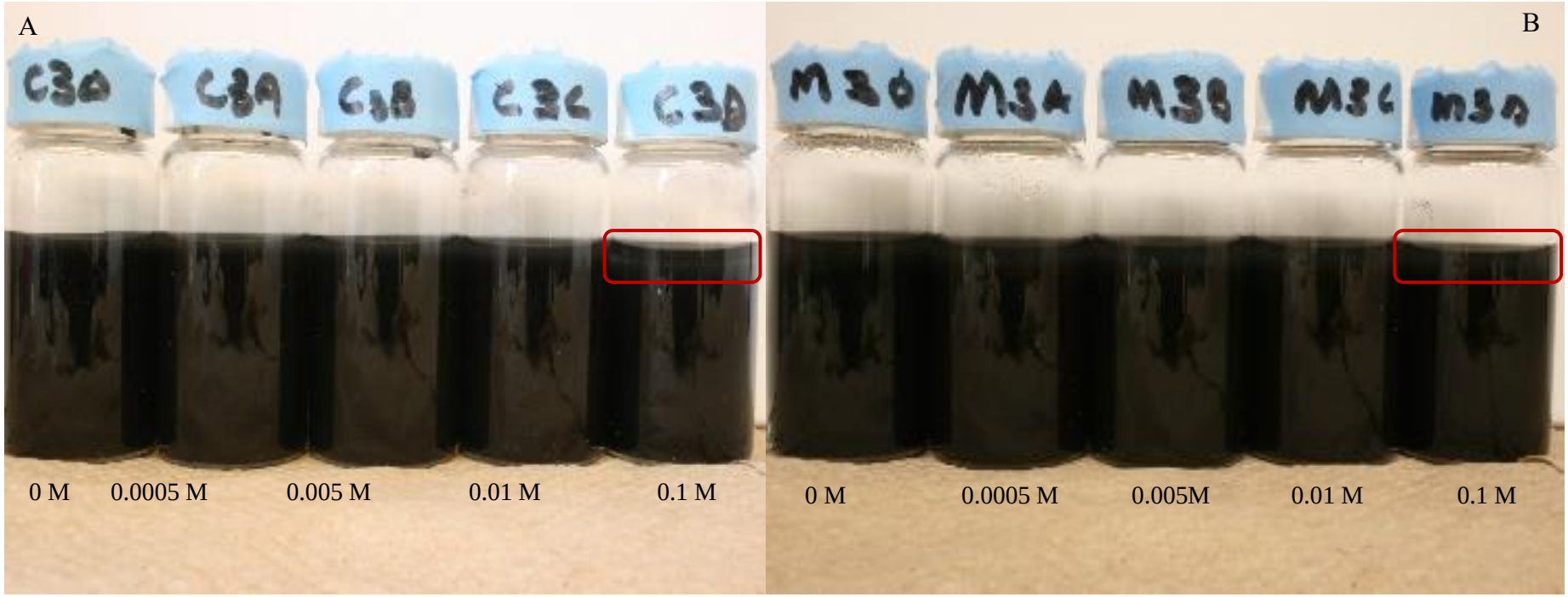

Fig. S9: Visual observations of aggregation and sedimentation of 0.025% CAC at 40 minutes in the presence of (A) $CaCl_2$ (B) NaCl

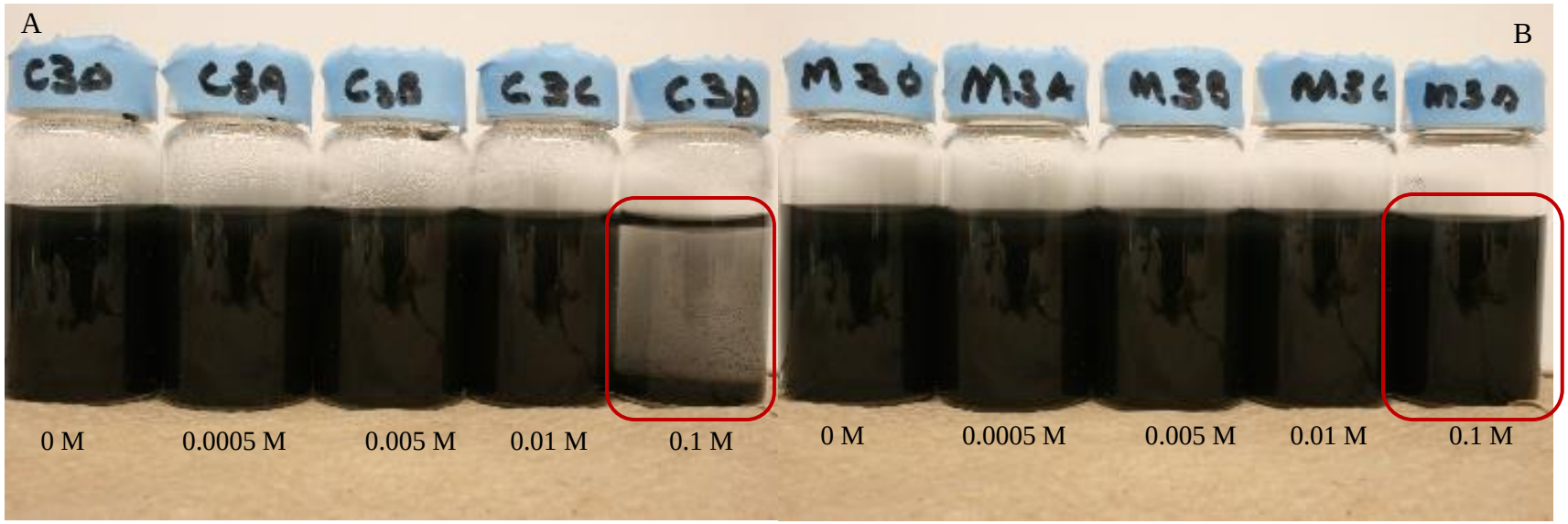

Fig. S10: Visual observations of aggregation and sedimentation of 0.025% CAC at 7 hours in the presence of (A) $CaCl_2$ (B) NaCl

S5. Adsorption of cations and DOM on CAC

The adsorption of cations and DOM on CAC was measured using the one-point sorption batch experiment adapted from [13]. Briefly, 25 mL suspension of 0.0115% CAC was prepared in triplicates by adding appropriate volumes of stock solutions of HA, BSA, Na^+, K^+, Mg^{2+}, or Ca^{2+} in 50 ml conical centrifuge tubes (Corning™ Falcon™). Then, the tubes were mounted on the wrist-action shaker for equilibration over 72 hours. After 72 hours, pH of samples was measured and then the tubes were centrifuged (Sorvall® RC-5C Plus Superspeed Centrifuge) at 10000 rpm for 20 minutes. Samples were carefully collected with 50-mL syringes and filtered with 0.2 μm Nylon (Basix™) filters for the DOM samples and 0.1 μm PDVF (Celltreat®) filters for cations. Filtered DOM samples were immediately analyzed, after appropriate dilution, for dissolved organic carbon (mg_c/L) using a persulfate wet oxidation method as described in Standard Method 5310D [14] with an O-I Corporation Model 1010 TOC Analyzer (College Station, Texas, USA). The filtered cation samples were diluted with nitric acid and stored at 4 °C until analyzed by inductively coupled plasma - optical emission spectrometry (iCAP™ Pro, Thermo Scientific™). The adsorbed amount of DOM and cations q_e (mg_c/g) was calculated using Eq. 1.

$$q_e\,(mg/g) = \frac{(C_0 - C_e)V}{m} \quad (1)$$

Where C_o and C_e are DOM or cation concentrations (mg_c/L) at time 0 h and at equilibrium, respectively; V = volume of solution (L) and m = mass of CAC (g).

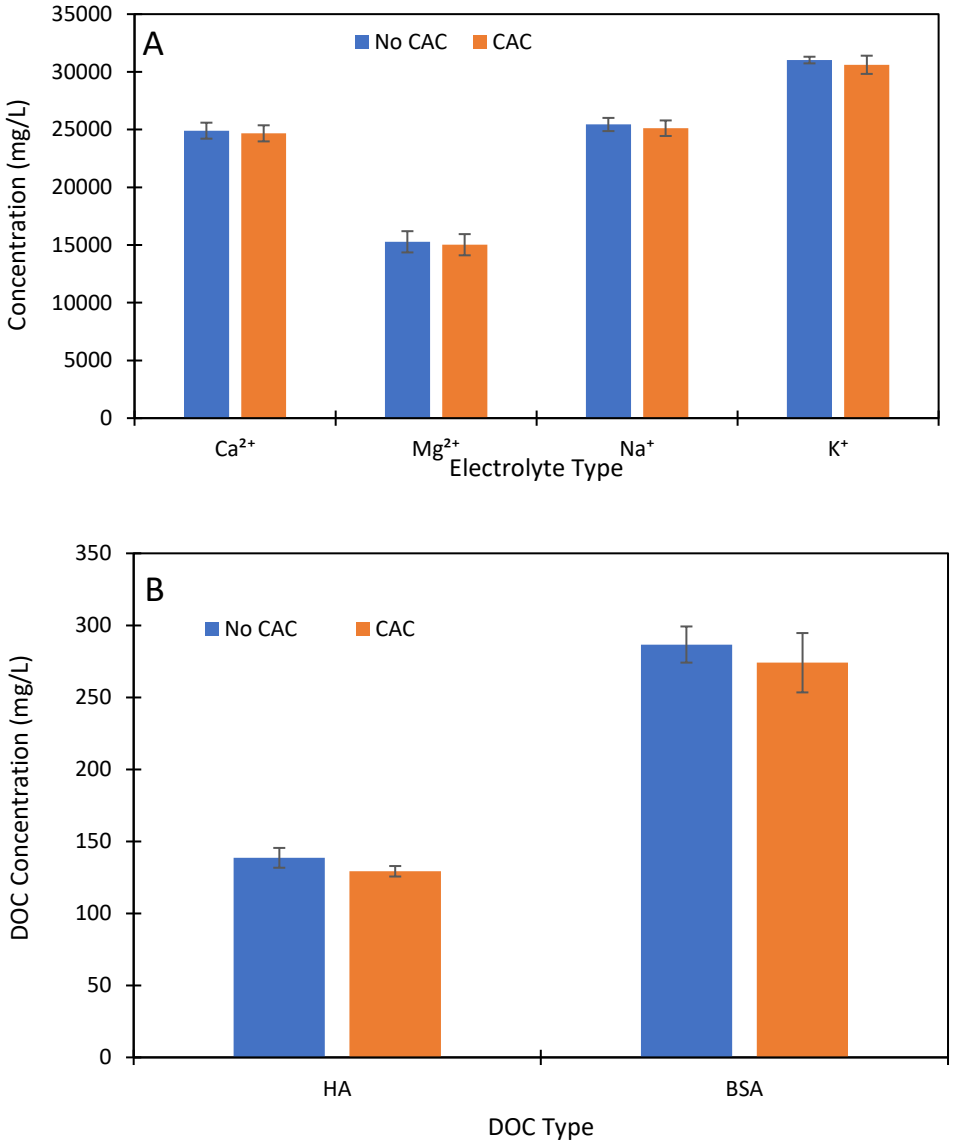

Fig. S11: Sorption on CAC (0.0115%) at a pH ~7 (A) cations where q_e (mg/g) is 0 for all the cations and (B) DOM where q_e (mg/g) is 100 ± 16.7 for HA and 0 for BSA.

S6. PZC and IEP of Polymer-free CAC

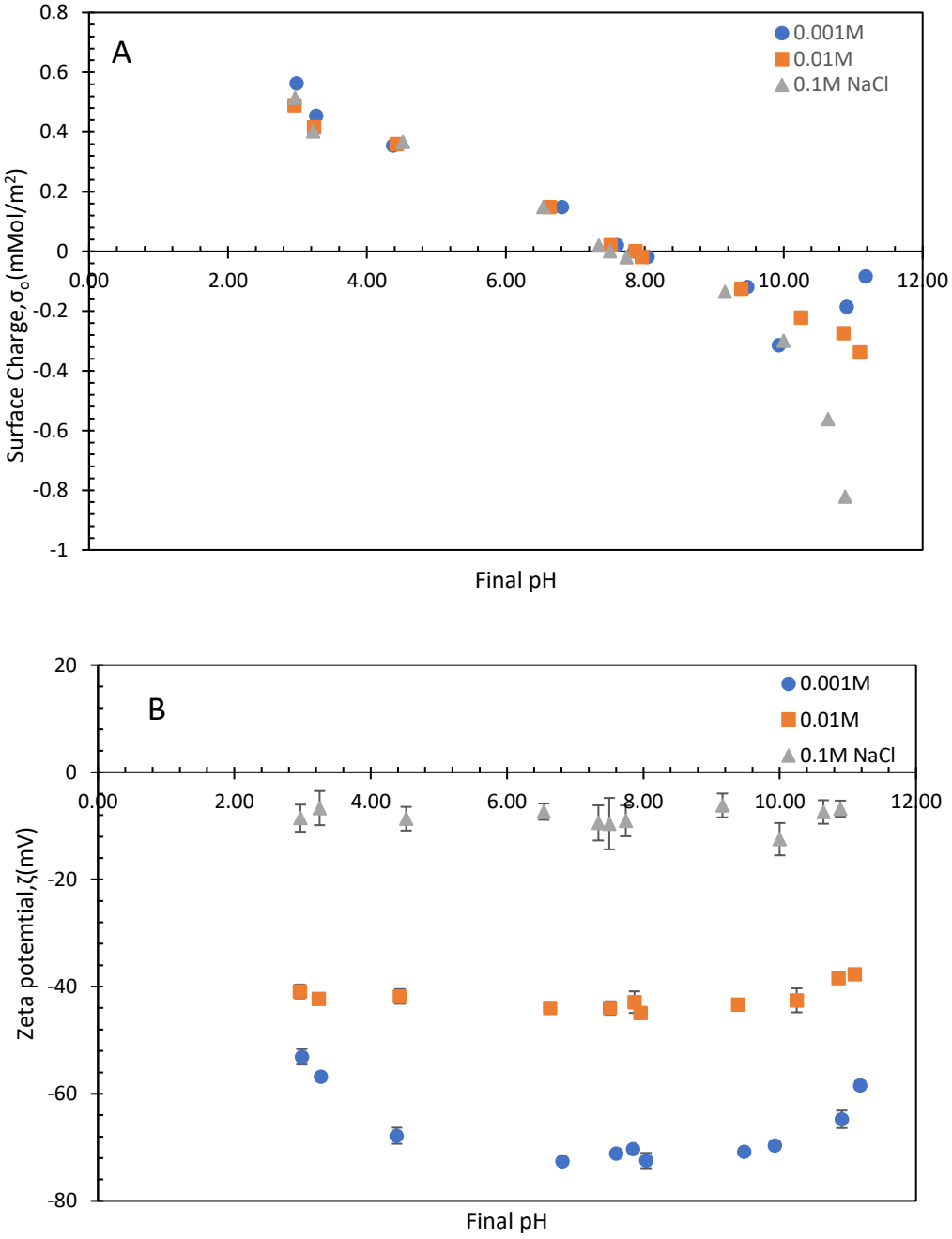

Fig. S12: Potentiometric charging curves for (A) PZC of polymer-free CAC as a function of pH and surface charge, with no sharp CIP and PZC 7.2-8.0 and (B) IEP of polymer-free CAC as a function of pH and ζ-potential, no charge reversal to show points of ζ-potential = 0 or extrapolated CIP, IEP <2.

S7. Sedimentation kinetic models for CAC

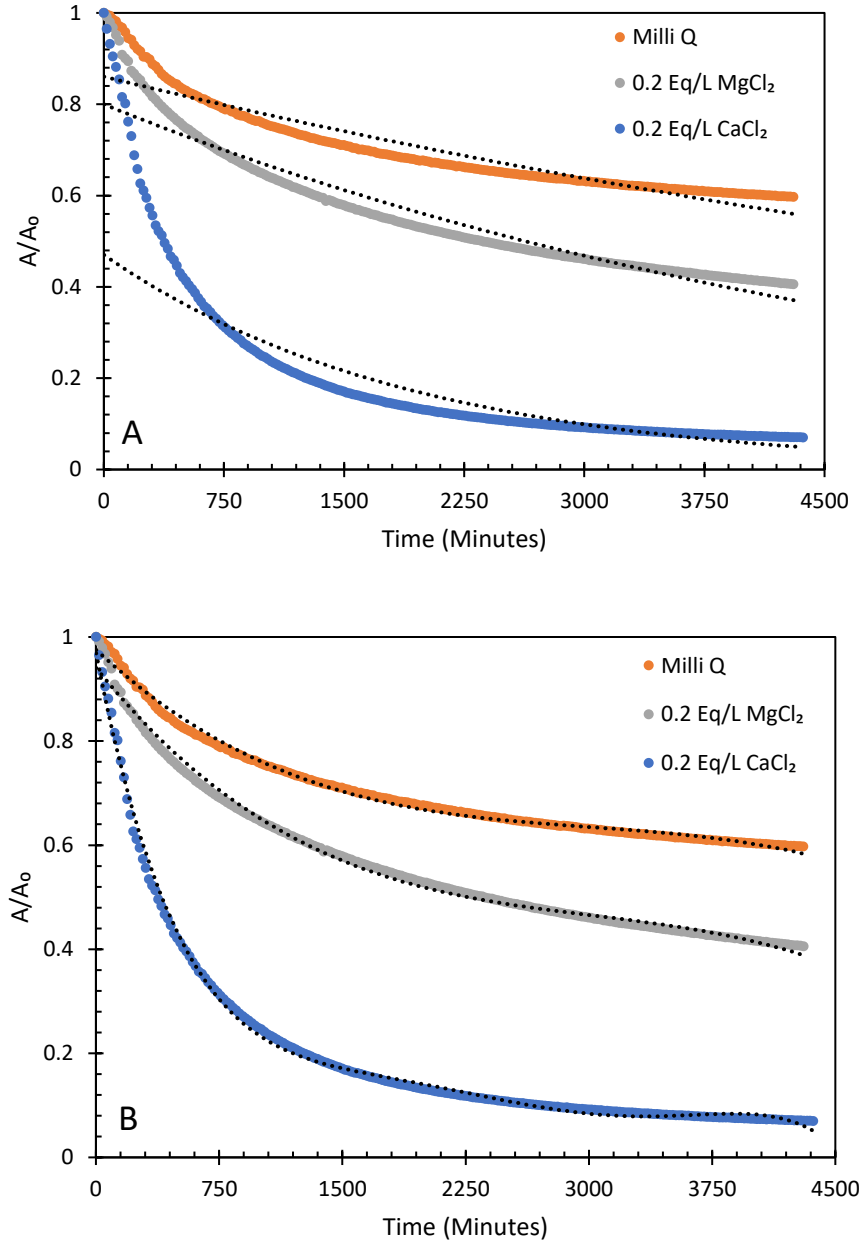

Fig. S13: Sedimentation kinetics for CAC at pH ~8. Dotted lines are the model fits for (A) Monophasic model ($^{C_t}/_{C_0} = M\,exp(Rt)$ where R^2 = 0.89-0.93 and (B) Biphasic Model ($^{C_t}/_{C_0} = M_1\,exp(R_1 t) + M_2\,exp(R_2 t)$ where R^2 = >0.99.

S8. Sedimentation kinetics parameters for various experimental conditions tested for 0.0115% CAC using UV-VIS

Table S7: Settling rate constants (R) and settled fractions (M) in the rapid and slow regimes of CAC sedimentation at varying pH conditions, calculated from the biphasic rate model (R^2 >0.99).

Background solution	pH	M_1	R_1 (Min^{-1})	M_2	R_2 (Min^{-1})
Milli-Q Water	9	0.299	-0.00157	0.699	-6.18E-05
	8	0.306	-0.00144	0.689	-5.22E-05
	7	0.303	-0.00146	0.696	-5.79E-05
	5	0.324	-0.00152	0.681	-6.23E-05
	4	0.329	-0.00153	0.679	-6.81E-05
	3	0.323	-0.00145	0.662	-7.14E-05

Table S8: Settling rate constants (R) and settled fractions (M) in the rapid and slow regimes of CAC sedimentation for various DOM type and concentrations, calculated from the biphasic rate model (R^2 >0.99).

Background solution	Concentration (mg C/L)	pH	M_1	R_1 (Min^{-1})	M_2	R_2 (Min^{-1})
BSA	1.9	7.78±0.4	0.309	-0.00151	0.682	-6.36E-05
	6		0.327	-0.00140	0.666	-5.77E-05
	10		0.322	-0.00142	0.667	-5.84E-05
	15		0.317	-0.00143	0.675	-5.55E-05
	22		0.324	-0.00139	0.666	-5.61E-05
HA	1.9	7.78±0.4	0.311	-0.00145	0.688	-5.71E-05
	6		0.300	-0.00151	0.699	-5.65E-05
	10		0.294	-0.00138	0.701	-4.91E-05
	15		0.285	-0.00137	0.710	-4.37E-05
	22		0.271	-0.00141	0.725	-3.92E-05

Table S1: Settling rate constants (R) and settled fractions (M) in the rapid and slow regimes of CAC sedimentation for various cation type/concentrations under an acidic or basic pH, calculated from the biphasic rate model (R^2 >0.99).

Background solution	**Concentration (eq/L)**	**pH**	**M_1**	**R_1 (Min^{-1})**	**M_2**	**R_2 (Min^{-1})**
K^+	0.001	7.69 ± 0.4	0.313	-0.00147	0.681	-6.15E-05
	0.005		0.325	-0.00153	0.676	-5.48E-05
	0.025		0.328	-0.00155	0.672	-6.72E-05
	0.05		0.334	-0.00151	0.662	-6.64E-05
	0.2		0.332	-0.00153	0.655	-7.22E-05
Na^+	0.001	7.69 ± 0.4	0.328	-0.00152	0.679	-6.21E-05
	0.005		0.332	-0.00163	0.683	-6.62E-05
	0.025		0.330	-0.00152	0.670	-6.56E-05
	0.05		0.329	-0.00160	0.670	-6.90E-05
	0.2		0.338	-0.00149	0.657	-6.91E-05
Mg^{2+}	0.001	7.69 ± 0.4	0.329	-0.00148	0.672	-6.41E-05
	0.005		0.327	-0.00164	0.675	-7.28E-05
	0.025		0.334	-0.00176	0.663	-8.74E-05
	0.05		0.335	-0.00183	0.660	-9.61E-05
	0.2		0.330	-0.00171	0.651	-1.15E-04
Ca^{2+}	0.001	7.69 ± 0.4	0.309	-0.00160	0.691	-6.62E-05
	0.005		0.319	-0.00156	0.670	-7.30E-05
	0.025		0.346	-0.00184	0.646	-1.05E-04
	0.05		0.414	-0.00198	0.583	-1.43E-04
	0.2		0.757	-0.00255	0.248	-3.17E-04
Na^+	0.001	3.1 ± 0.9	0.333	-0.00161	0.655	-7.24E-05
	0.005		0.337	-0.00152	0.644	-7.24E-05
	0.025		0.330	-0.00168	0.654	-8.07E-05
	0.05		0.336	-0.00175	0.652	-8.50E-05
	0.2		0.364	-0.00199	0.625	-1.16E-04
Ca^{2+}	0.001	3.1 ± 0.9	0.335	-0.00157	0.649	-7.49E-05
	0.005		0.334	-0.00177	0.650	-8.52E-05
	0.025		0.431	-0.00238	0.547	-1.65E-04
	0.05		0.619	-0.00266	0.350	-1.58E-04
	0.2		0.935	-0.00542	0.063	-4.14E-04

Table S2: Settling rate constants (R) and settled fractions (M) in the rapid and slow regimes of CAC sedimentation for combined effects of Na^+ and DOM, calculated from the biphasic rate model (R^2 >0.99) model.

Background solution	**Cation concentration (eq/L)**	**DOM concentration (mg_C/L)**	**pH**	**M_1**	**R_1 (Min^{-1})**	**M_2**	**R_2 (Min^{-1})**
Na^+-HA	0.001	1.9	7.45 ± 0.3	0.318	-0.00140	0.676	-5.84E-05
	0.005			0.337	-0.00154	0.656	-6.27E-05
	0.025			0.337	-0.00155	0.662	-6.61E-05
	0.05			0.330	-0.00152	0.661	-6.69E-05
	0.2			0.335	-0.00151	0.654	-6.98E-05
	0.001	6		0.299	-0.00149	0.693	-6.05E-05
	0.005			0.303	-0.00141	0.691	-5.61E-05
	0.025			0.315	-0.00146	0.672	-5.74E-05
	0.05			0.316	-0.00146	0.370	-6.15E-05
	0.2			0.314	-0.00148	0.675	-6.65E-05
	0.001	10		0.292	-0.00148	0.697	-5.69E-05
	0.005			0.320	-0.00130	0.672	-4.66E-05
	0.025			0.310	-0.00146	0.682	-5.58E-05
	0.05			0.317	-0.00144	0.677	-5.88E-05
	0.2			0.310	-0.00148	0.682	-6.45E-05
Na^+-BSA	0.001	1.9		0.315	-0.00156	0.655	-6.68E-05
	0.005			0.182	-0.00143	0.651	-6.28E-05
	0.025			0.340	-0.00144	0.648	-6.47E-05
	0.05			0.344	-0.00140	0.648	-6.50E-05
	0.2			0.352	-0.00137	0.634	-6.16E-05
	0.001	6		0.334	-0.00137	0.656	-6.39E-05
	0.005			0.341	-0.00146	0.652	-3.82E-05
	0.025			0.346	-0.00161	0.643	-8.81E-05
	0.05			0.367	-0.00174	0.620	-1.10E-04
	0.2			0.428	-0.00180	0.558	-1.79E-04
	0.001	10		0.292	-0.00148	0.697	-5.69E-05
	0.005			0.320	-0.00130	0.672	-4.66E-05
	0.025			0.310	-0.00146	0.682	-5.58E-05
	0.05			0.317	-0.00144	0.677	-5.88E-05
	0.2			0.310	-0.00148	0.682	-6.45E-05

Table S3: Settling rate constants (R) and settled fractions (M) in the rapid and slow regimes of CAC sedimentation for combined effects of Ca^{2+} and DOM, calculated from the biphasic rate model (R^2 >0.99).

Background solution	**Cation concentration (eq/L)**	**DOM concentration (mg_C/L)**	**pH**	**M_1**	**R_1 (Min^{-1})**	**M_2**	**R_2 (Min^{-1})**
Ca^{2+}-HA	0.001	1.9	7.45 ± 0.3	0.324	-0.00144	0.666	-6.08E-05
	0.005			0.324	-0.00150	0.667	-7.22E-05
	0.025			0.456	-0.00157	0.524	-1.63E-04
	0.05			0.711	-0.00291	0.274	-3.35E-04
	0.2			0.922	-0.00616	0.115	-6.02E-04
	0.001	6		0.324	-0.00144	0.666	-6.08E-05
	0.005			0.324	-0.00150	0.667	-7.22E-05
	0.025			0.901	-0.00483	0.160	-2.83E-04
	0.05			1.003	-0.00858	0.077	-4.33E-03
	0.2			0.999	-0.01075	0.092	-1.10E-03
	0.001	10		0.301	-0.00145	0.690	-5.78E-05
	0.005			0.464	-0.00087	0.522	-5.93E-05
	0.025			0.986	-0.00827	0.093	-3.94E-04
	0.05			1.047	-0.01042	0.057	-8.18E-04
	0.2			1.028	-0.01124	0.065	-1.24E-03
Ca^{2+}-BSA	0.001	1.9		0.334	-0.00145	0.656	-6.71E-05
	0.005			0.332	-0.00146	0.658	-7.01E-05
	0.025			0.337	-0.00159	0.650	-8.19E-05
	0.05			0.352	-0.00166	0.633	-1.04E-04
	0.2			0.623	-0.00202	0.354	-3.08E-04
	0.001	6		0.334	-0.00137	0.656	-6.39E-05
	0.005			0.341	-0.00146	0.652	-6.91E-05
	0.025			0.346	-0.00161	0.643	-8.81E-05
	0.05			0.366	-0.00171	0.619	-1.09E-04
	0.2			0.428	-0.00180	0.556	-1.79E-04
	0.001	10		0.339	-0.00138	0.656	-5.88E-05
	0.005			0.330	-0.00151	0.661	-7.31E-05
	0.025			0.339	-0.00159	0.642	-9.06E-05
	0.05			0.356	-0.00167	0.628	-1.09E-04
	0.2			0.406	-0.00176	0.579	-1.70E-04

Table S4: Settling rate constants (R) and settled fractions (M) in the rapid and slow regimes of CAC sedimentation for various coagulants, calculated from the biphasic rate model (R^2 >0.99).

Background solution	**Concentration (eq/L)**	**pH**	**M_1**	**R_1 (Min^{-1})**	**M_2**	**R_2 (Min^{-1})**
Al^{3+} ($AlCl_3$)	0.001	3.1 ± 0.9	0.352	-0.00162	0.646	-7.39E-05
	0.05		0.575	-0.00164	0.410	-3.27E-03
Fe^{3+}	0.001		0.334	-0.00144	0.670	-6.42E-05
	0.05		0.681	-0.00139	0.285	-7.34E-05
Al^{3+} ($Al_2(SO_4)_3$)	0.001		-0.021	0.00015	1.133	-8.34E-03
	0.05		-0.020	0.00018	1.106	-9.27E-03

S9. Relationship between short- and long-term stability of CAC

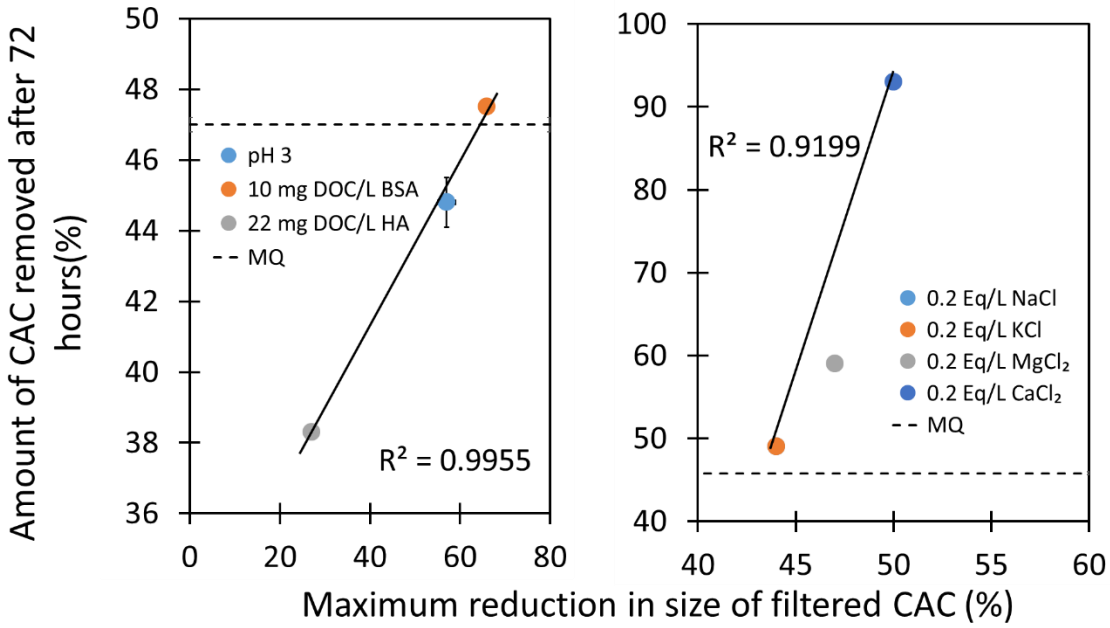

Fig. S14: Relationship between short-term stability and long-term stability of CAC. (A) Steric stabilization conditions (B) Cation-bridging conditions. Error bars show standard deviation, n=6 for X-axis and n=2 for Y-axis.

S10. Effect of cation type and concentration on sedimentation and aggregation kinetics of CAC

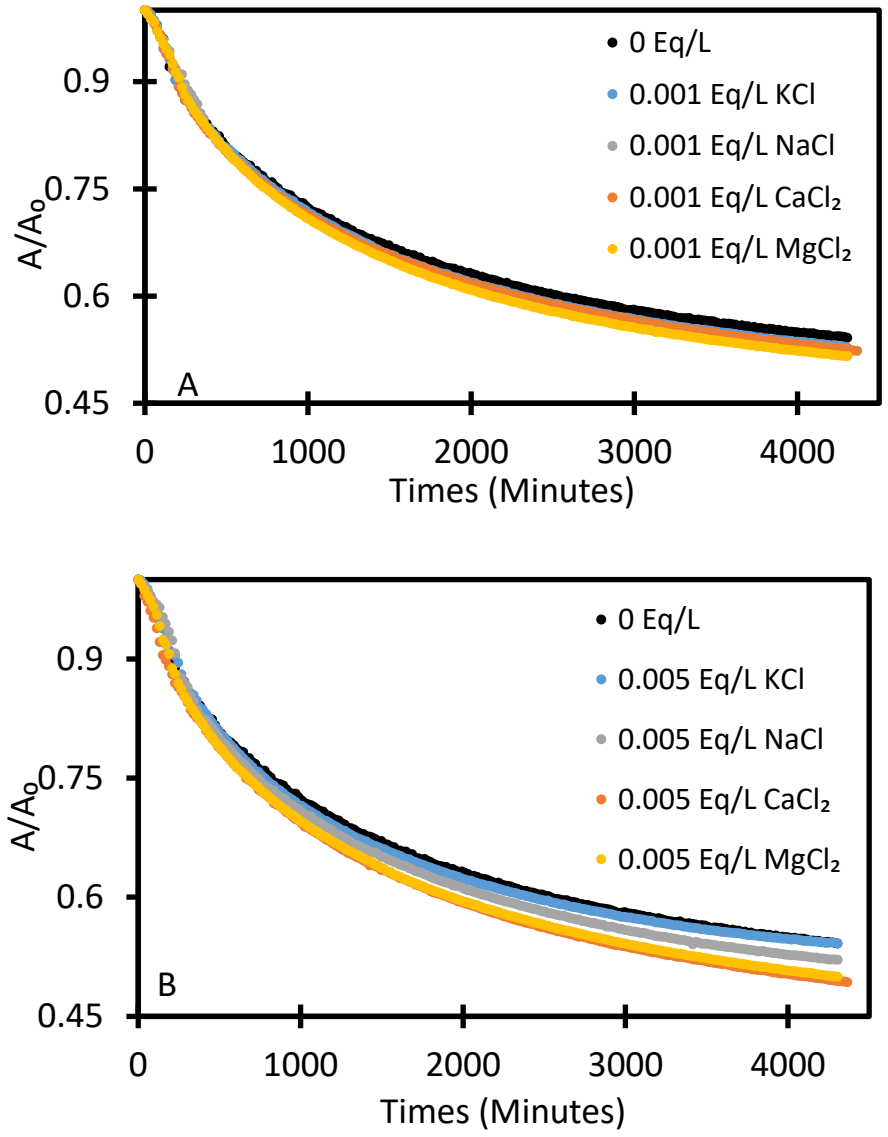

Fig. S15 Sedimentation kinetics profile of CAC as a function of cation type and concentration (A) 0.001 Eq/L and (B) 0.005 Eq/L over 72 hours at pH 7.69 ± 0.4.

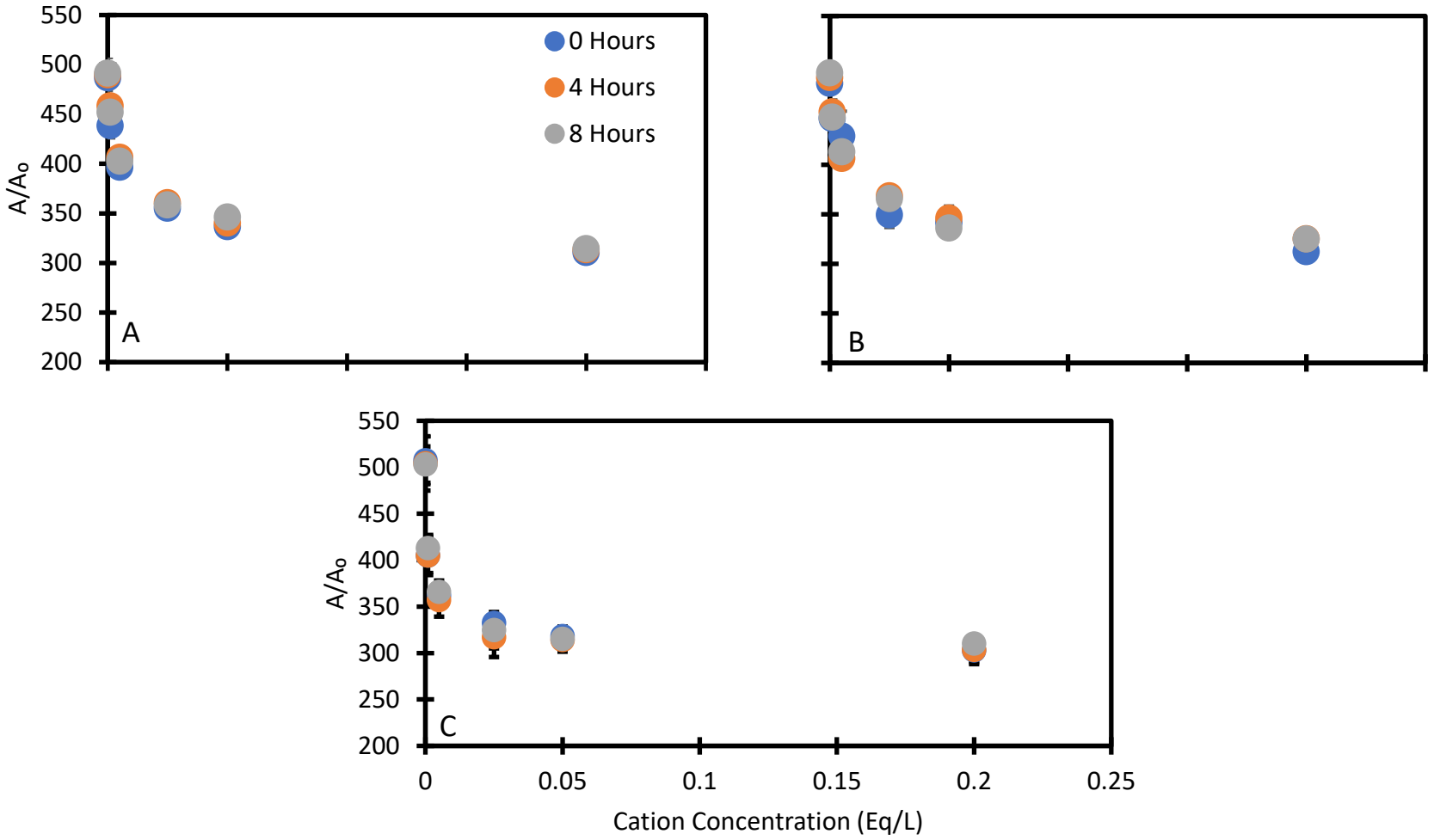

Fig. S16: Aggregation kinetics of CAC in the presence of various types of cations at (A) KCl, (B) NaCl, and (C) $MgCl_2$. Measurements were taken at filtered 0.024% CAC (Dz = 472.444 ± 35.5 nm).

S11. Comparison of the observed order for the effect of mono- and di- valent cations on CAC stability to common specific ion effect theories

Table S13: Possible explanation for SIE: standard direct HF series, atomic mass, ionic radius, hydration radius, hydration energy. *applies to divalent cations only

<table>
<tr><th colspan="2">HF series</th><th rowspan="2">Current study</th></tr>
<tr><th>HF series (order of stabilization of colloids)</th><th>Reference</th></tr>
<tr><td>$N(CH_3)_4^+ > NH_4^+ > Cs^+ > Rb^+ > K^+ > Na^+ > Li^+ > Mg^{2+} > Ca^{2+}$</td><td>15–19</td><td rowspan="10">At concentrations < 0.025 Eq/L ➔ $K^+ = Na^+ = Mg^{2+} = Ca^{2+}$
At concentrations ≥ 0.025 Eq/L ➔ $K^+ = Na^+ > Mg^{2+} >> Ca^{2+}$</td></tr>
<tr><td>$Li^+ > K^+ \approx Na^+ > NH_4^+ > Mg^{2+}$</td><td>20</td></tr>
<tr><td>$N(CH_3)_4^+ > CH_3)_2NH_2^+ > NH_4^+ > K^+ > Na^+ > Cs^+ > Li^+ > Rb^+ > Mg^{2+} > Ca^{2+} > Ba^{2+}$</td><td>21,22</td></tr>
<tr><td>$N(CH_3)_4^+ > NH_4^+ > Cs^+ > Rb^+ > K^+ > Na^+ > Li^+ > Ca^{2+} > Mg^{2+}$</td><td>23</td></tr>
<tr><td>$N(CH_3)_4^+ > NH_4^+ > Cs^+ > Rb^+ > K^+ > Na^+ > H^+ > Ca^{2+} > Mg^{2+}$</td><td>24</td></tr>
<tr><td>$Cs^+ > Rb^+ > NH_4^+ > K^+ > Na^+ > Li^+ > Ba^{2+} > Sr^{2+} > Ca^{2+} > Mg^{2+}$</td><td>25</td></tr>
<tr><td colspan="2">variation atomic mass/ionic radius/hydration radius/hydration energy</td></tr>
<tr><td>$aggregation\ \alpha\ relative\ atomic\ mass$
$Na^+ > Mg^{2+} > Ca^{2+} > Sr^{2+} > Ba^{2+}$</td><td rowspan="2">26</td></tr>
<tr><td>$aggregation\ \alpha\ \frac{1}{hydration\ energy}$ *
$aggregation\ \alpha\ ionic\ radius$ *
$Mg^{2+} > Ca^{2+} > Sr^{2+} > Ba^{2+}$</td></tr>
<tr><td colspan="2">Hydrophobicity/hydrophilicity</td></tr>
</table>

Hydrophobic surface $Na^+ = Mg^{2+} = Sr^{2+} = Ca^{2+} = Ba^{2+}$ Hydrophilic surface $Na^+ \approx Mg^{2+} > Sr^{2+} > Ca^{2+} > Ba^{2+}$	[27]	

Table S14: Properties of ions used in this study. [a] adapted from (Marcus, 2015) [b]adapted from (Nightingale, 1959) [c] adapted from (Rosseinsky, 1965)

Ions	**Atomic mass (amu)[a]**	**Ionic radius (pm)[a]**	**Hydrated ion (pm) [b]**	**Hydration Energy (kJ/mol) [c]**	**Valence**
K^+	39.1	138	331	-334	1
Na^+	23.0	102	358	-416	
Mg^{2+}	24.3	72	428	-1949	2
Ca^{2+}	40.1	100	412	-1602	
Al^{3+}	27.0	53	475	-4715	3
Fe^{3+}	55.8	65	457	-4462	
Cl^-	35.5	181	332	-367	1
SO_4^{2-}	96.1	230	379	-1035	2

S12. Combined effect of Na^+-pH and Na^+-DOM on the sedimentation kinetics of CAC

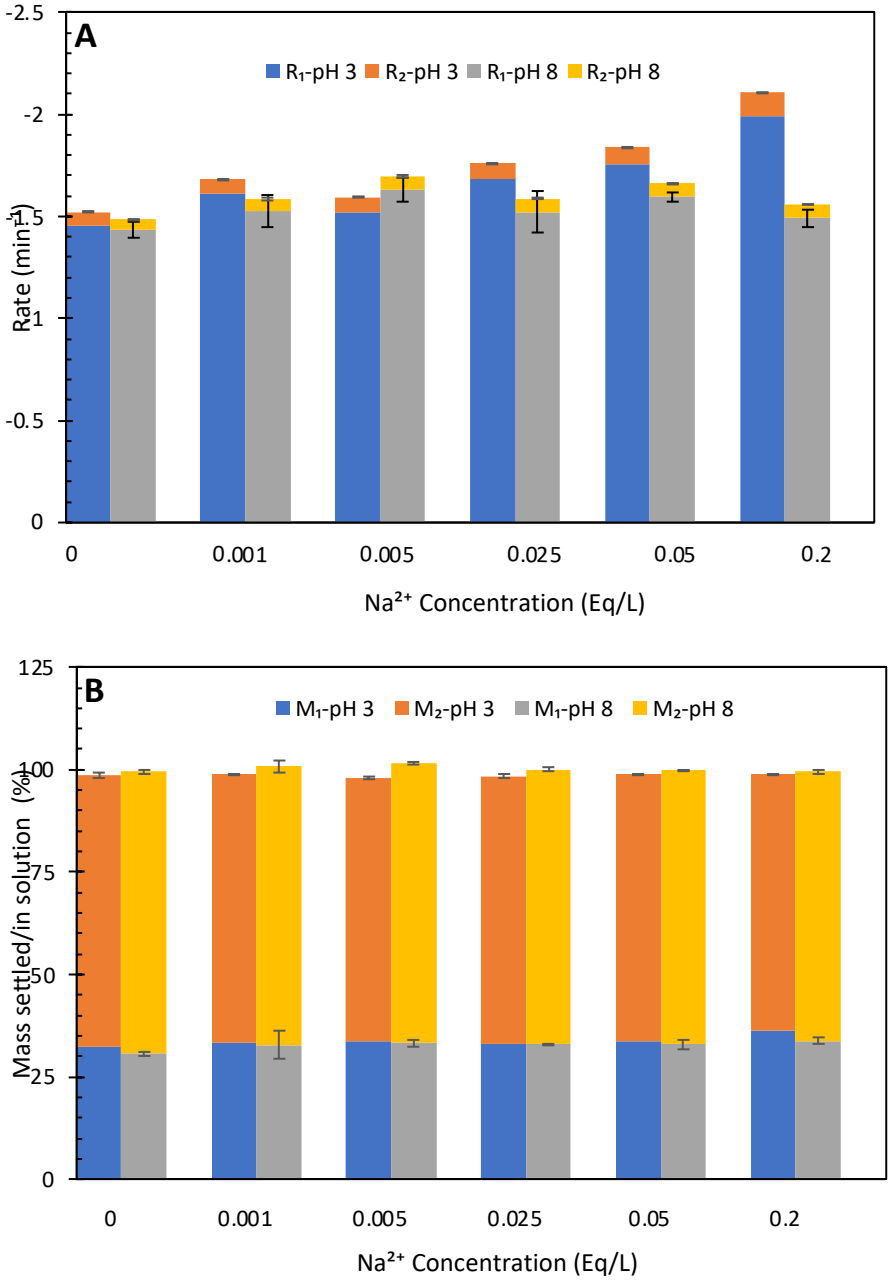

Fig. S17: Combined effects of Na^+ and pH on the sedimentation kinetics parameters (A) settling rate in fast regime (R_1) and in slow regime (R_2) and (B) mass settled in fast regime (M_1) and remaining in solution in slow regime (M_2).

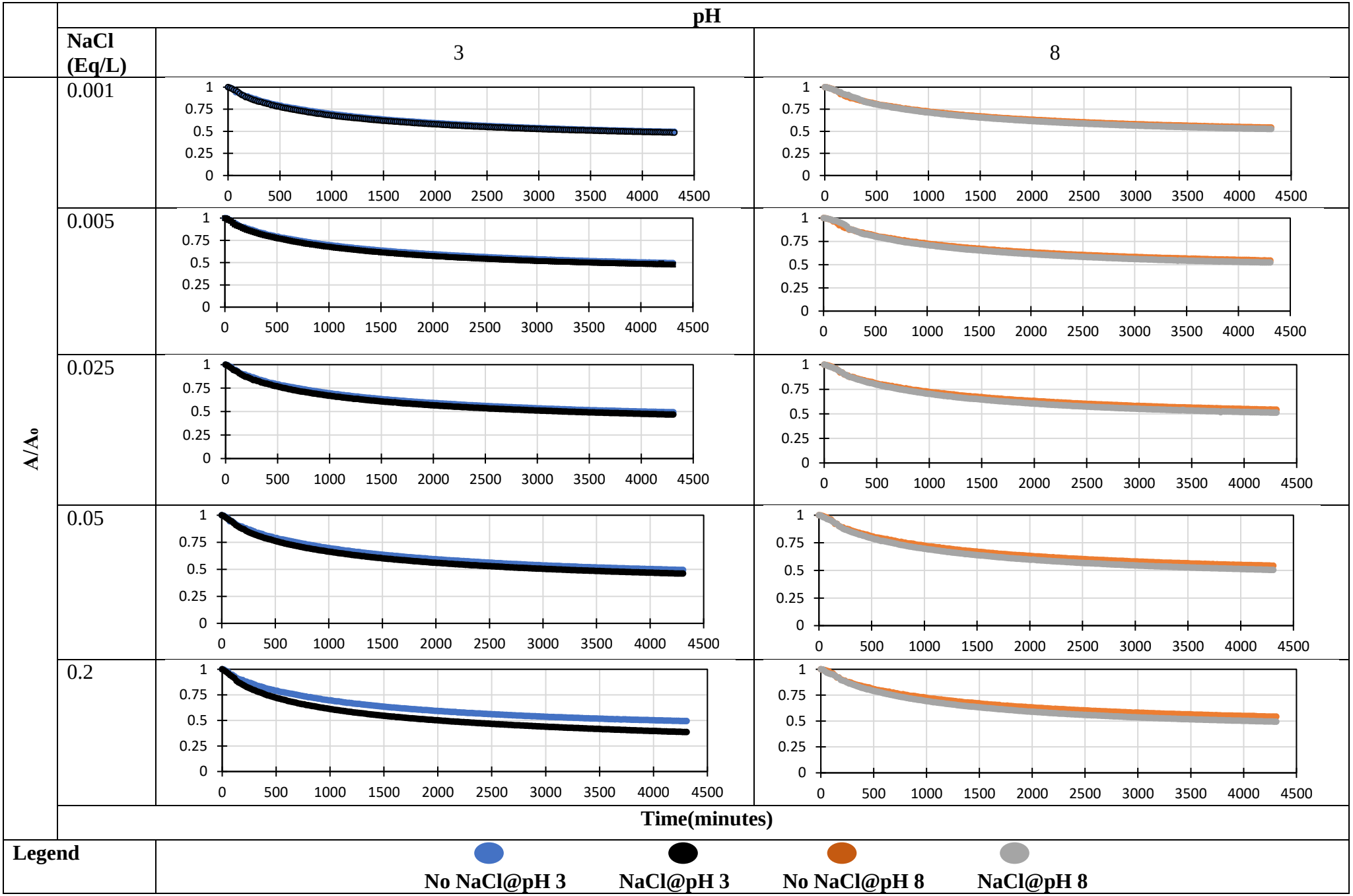

Fig. S18: Combined effect of Na^+ and pH on sedimentation kinetics of CAC over 72 hours at pH 7.72 ± 0.5 and 3.38 ± 0.05.

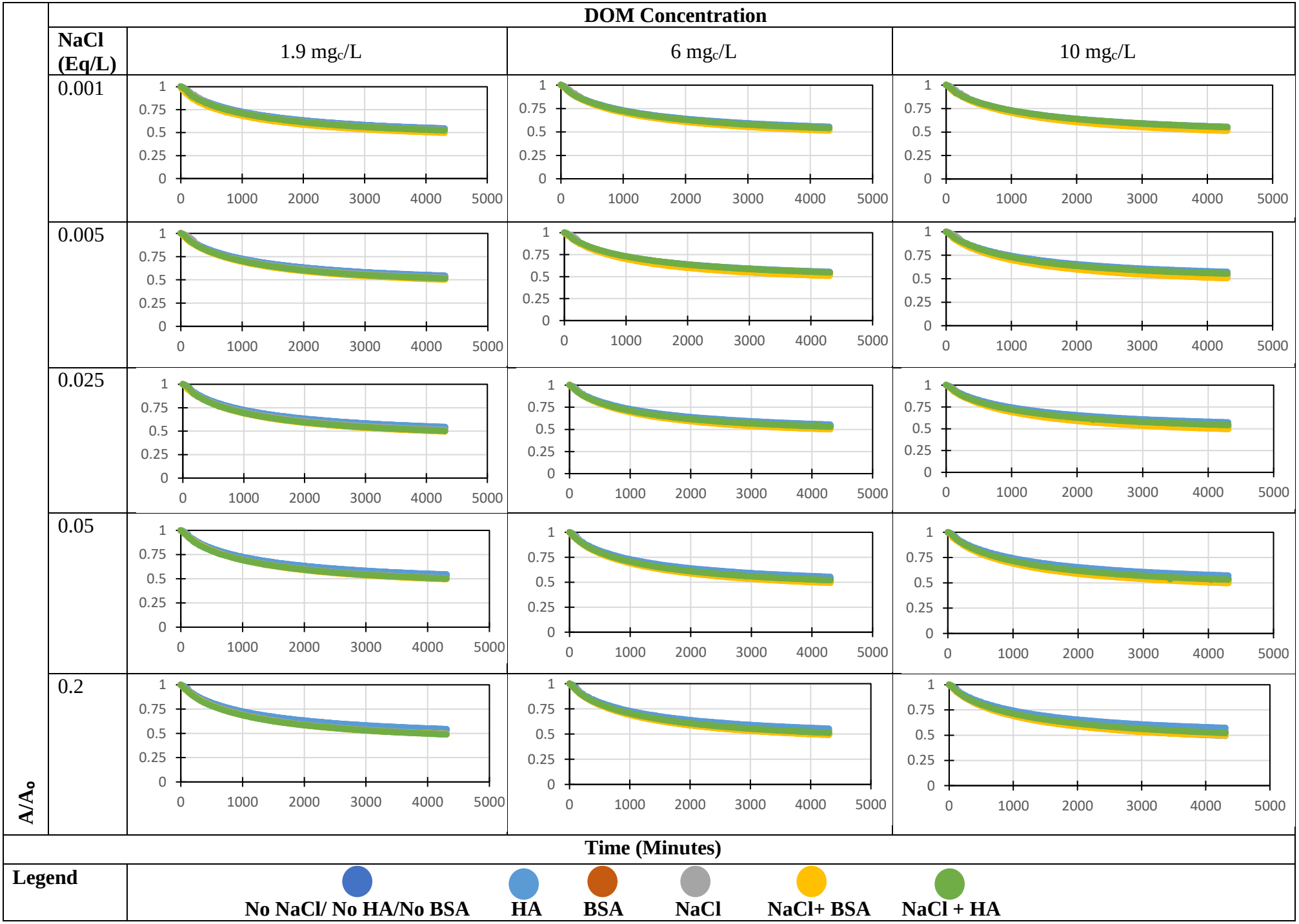

Fig. S19: Combined effect of Na^+ and DOM on the sedimentation kinetics of CAC over 72 hours at pH 7.44 ± 0.3.

S13. Combined effect of Ca^{2+}-pH and Ca^{2+}- DOM on the sedimentation kinetics of CAC

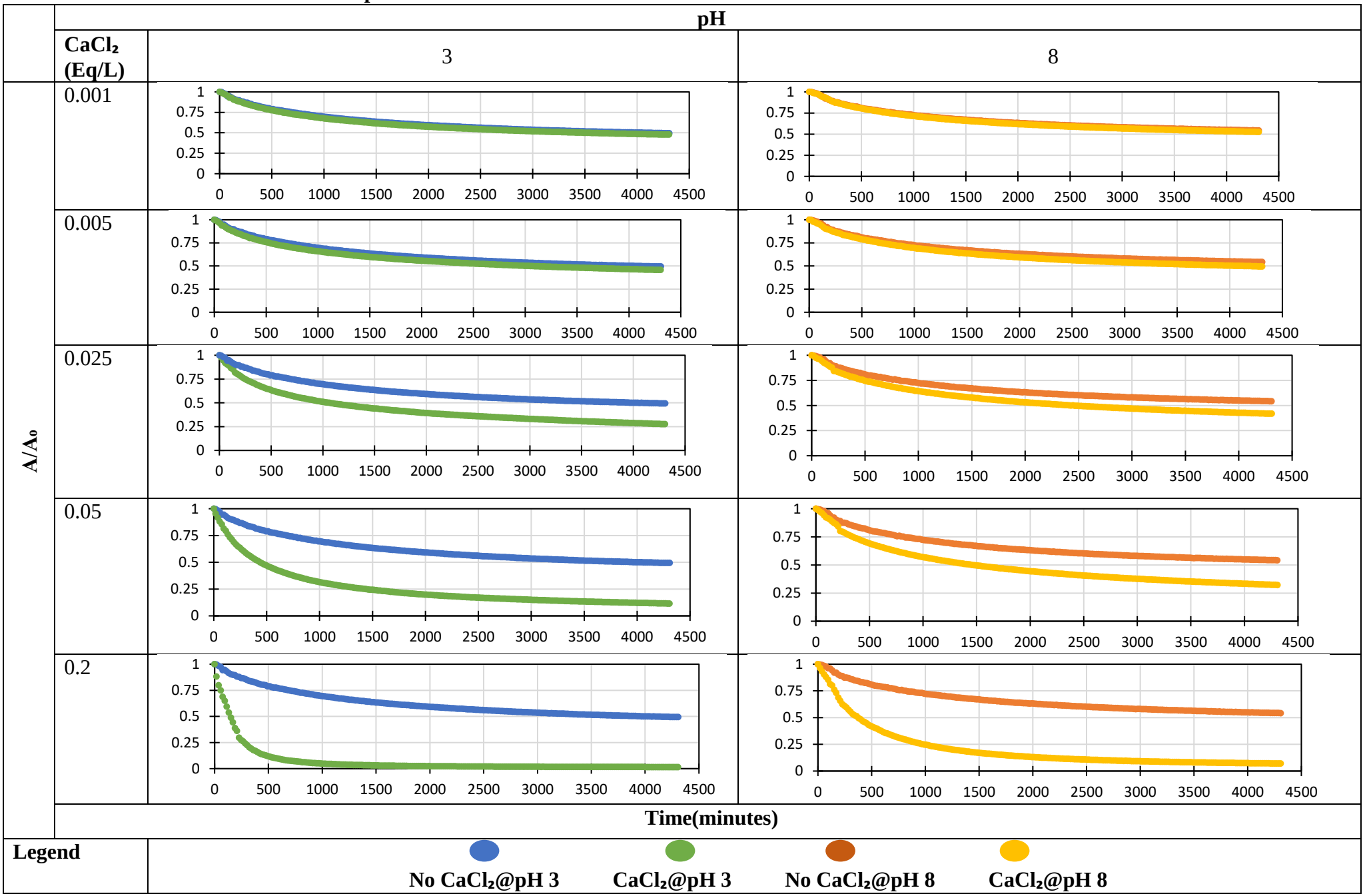

Figure S20: Combined effect of Ca^{2+} and pH on sedimentation kinetics of CAC over 72 hours at pH 7.72 ± 0.5 and 3.38 ± 0.05.

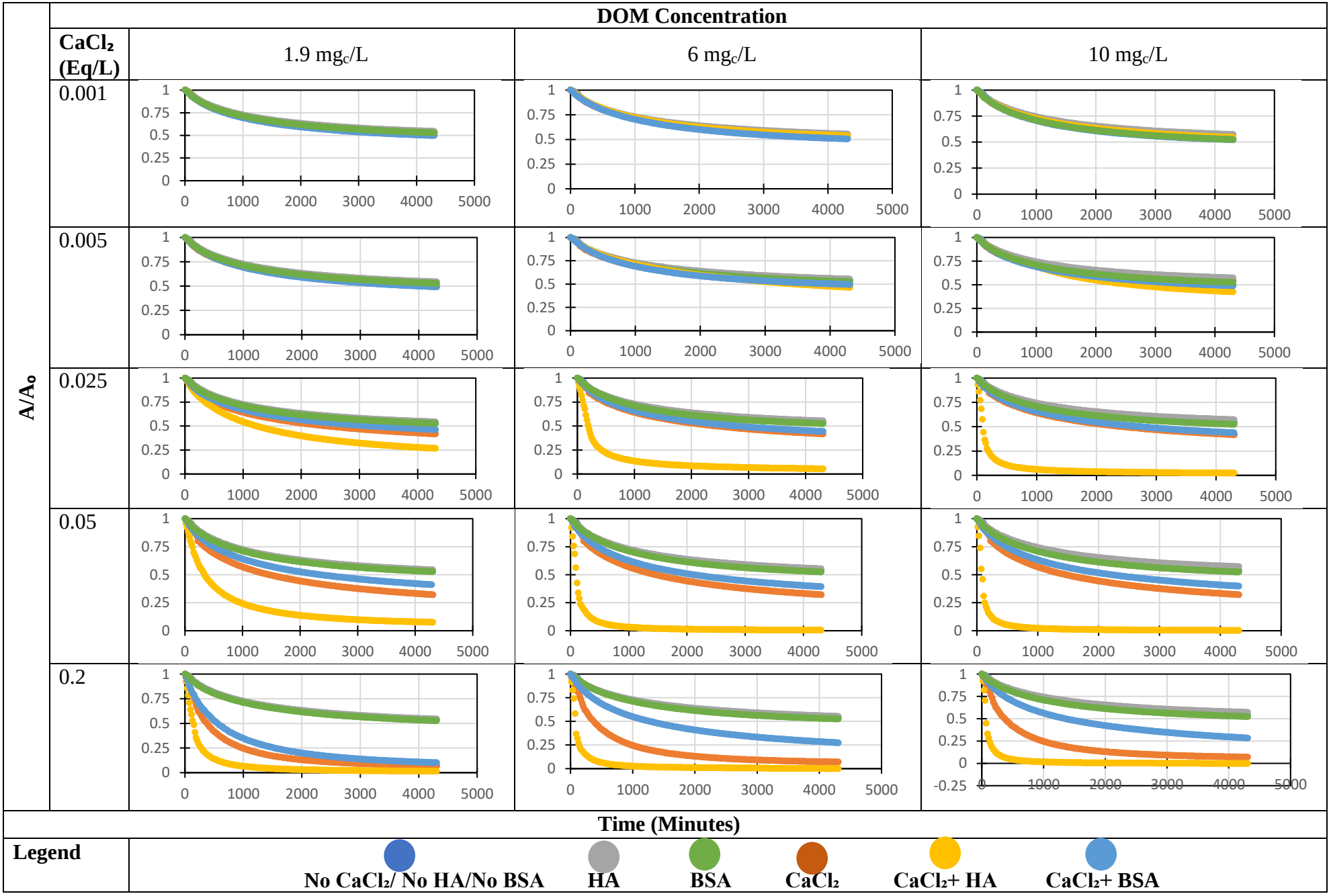

Fig. S21: Combined effect of Ca^{2+} and DOM (mg_c/L) on the sedimentation kinetics of CAC over 72 hours at pH 7.45 ± 0.3.

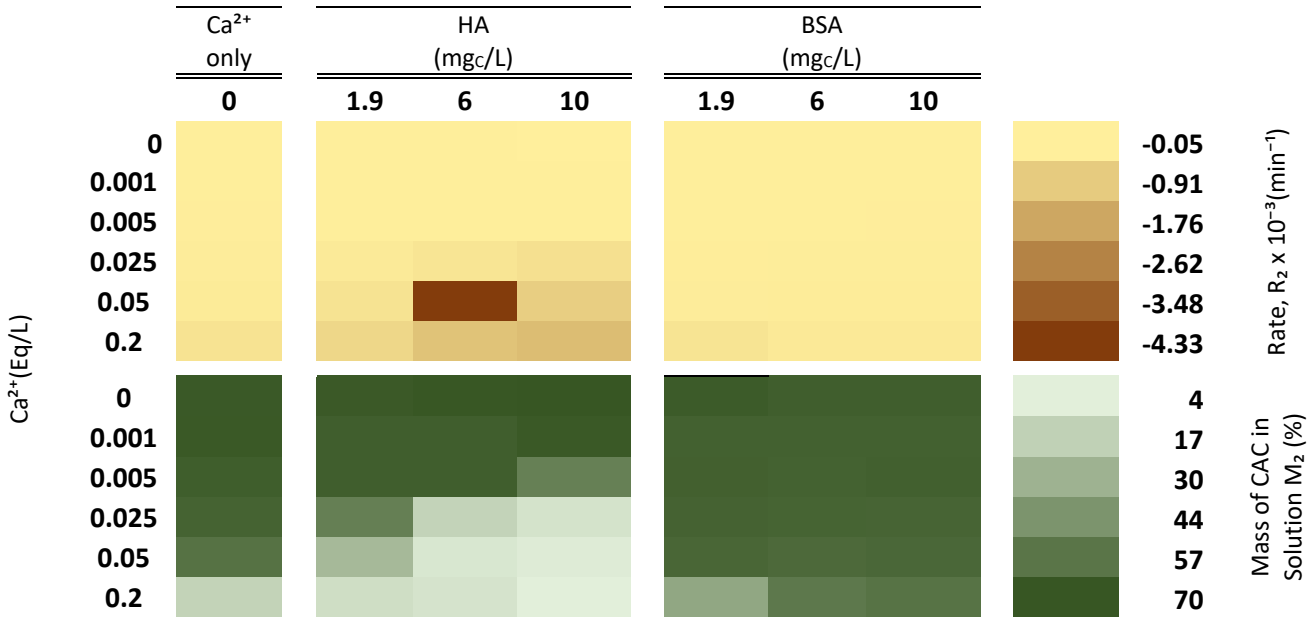

Fig. S22: Combined effect of Ca^{2+} (Eq/L) and DOM (mgc/L) on sedimentation kinetics parameters R_2 and $M_2$of CAC over 72 hours at pH 7.45 ± 0.3.

S14 Combined effect of Ca^{2+} and Na^{+} on the aggregation kinetics of CAC

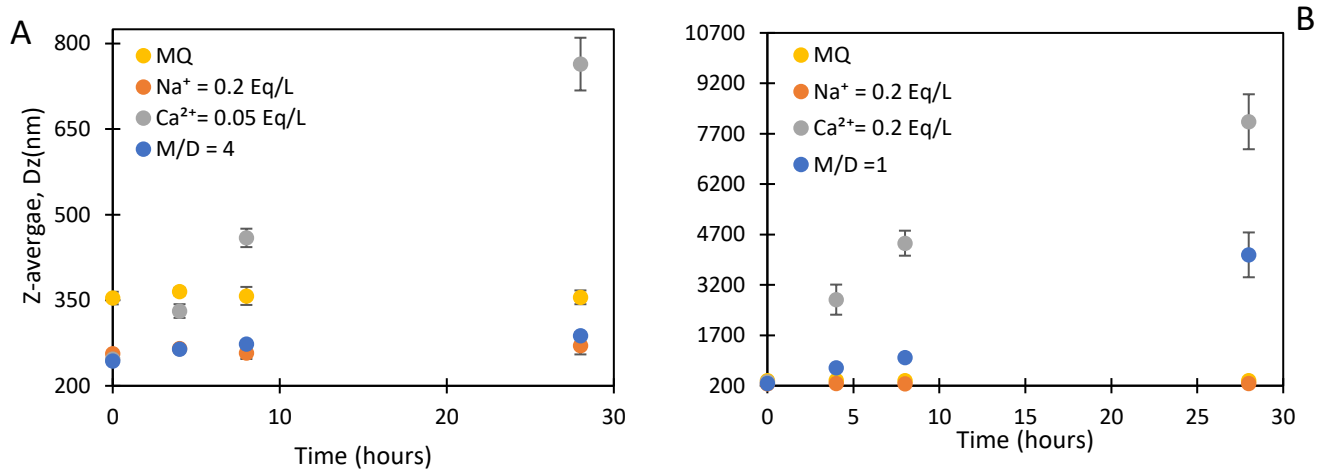

Fig. S23: Combined effect of Na^{+} and Ca^{2+} (M/D) on the aggregation kinetics of filtered CAC over 24 hours at pH~8. M/D is the ratio of Na^{+} to Ca^{2+}. (A) M/D = 4 and (B) M/D =1.

S16 CAC aggregation and sedimentation in real groundwater samples

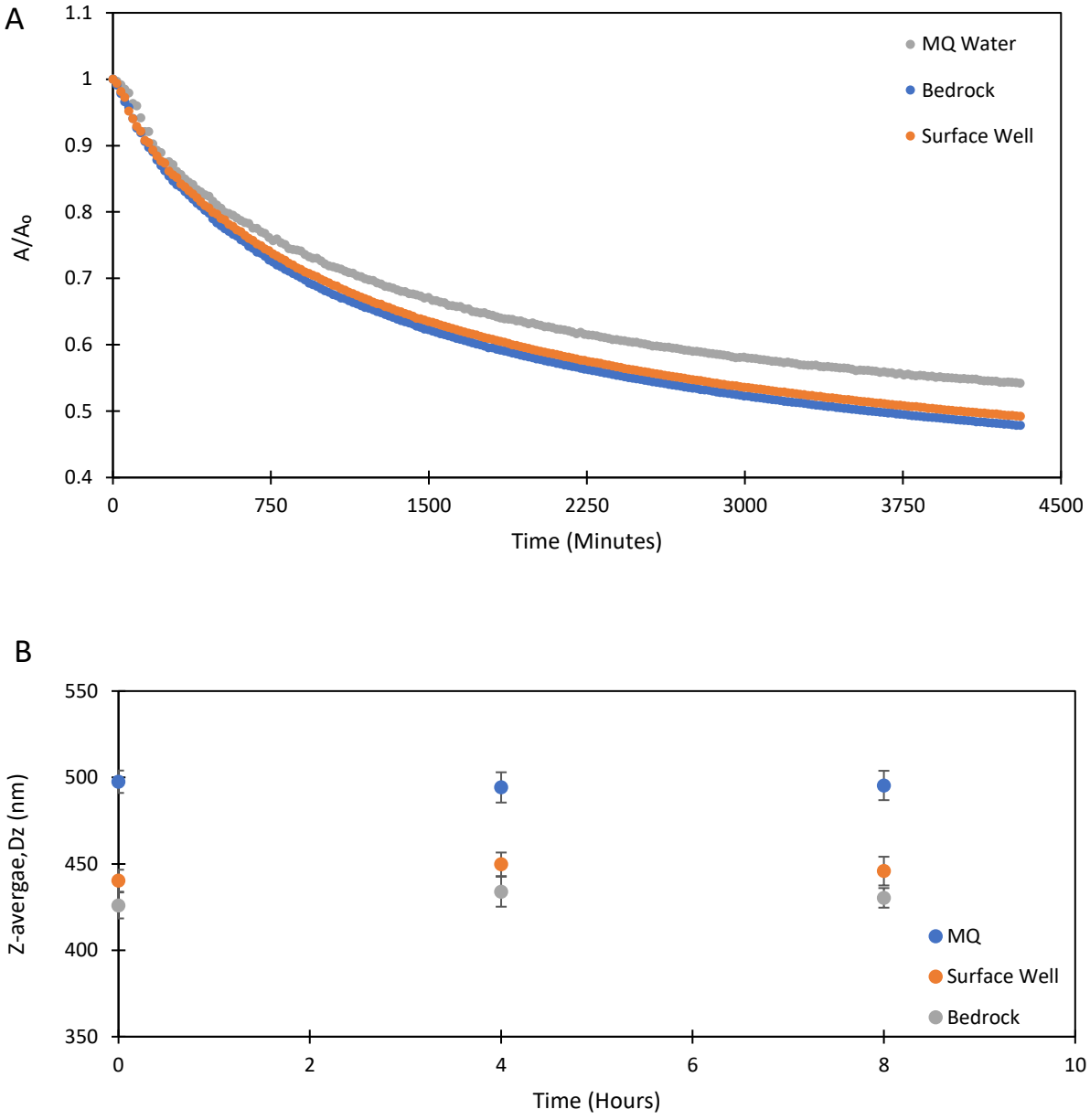

Fig. S24: Effect of groundwater samples on stability of CAC (A) sedimentation kinetics (B) aggregation kinetics

Table S 15: Chemical composition of groundwater samples

Parameter	Bed Rock	Surface well
pH	7.2	7.1
mg/L		
Ca^{2+}	74.8 ± 0.4	40.7 ± 11.4
Mg^{2+}	18 ± 0.06	8.4 ± 1
Na^{+}	13.2 ± 0.06	14.9 ± 1.7
K^{+}	3.6 ± 0.06	0.9 ± 0.1
Fe^{3+}	ND	ND
Al^{3+}	0.2 ± 0	0.2 ± 0
Cu^{2+}	ND	ND
DOC	0.6 ± 0.05	0.4 ± 0.06

References

1 K. Franks, A. Braun, J. Charoud-Got, O. Couteau, V. Kestens, A. Lamberty, T. P. J. Linsinger and G. Roebben, *Certification of the Equivalent Spherical Diameters of Silica Nanoparticles in Aqueous Solution Certified Reference Material ERM ® -FD304*, 2012.

2 Horiba, *Colloidal Silica as a Partical Szie and Charge Refrence Material*, 2009.

3 Grace Materials Technologies, LUDOX ® TM-50 product information, https://www.chempoint.com/products/download?grade=5213&doctype=tds, (accessed 18 April 2023).

4 R. W. O'Brien and L. R. White, *J. Chem. Soc. Faraday Trans. 2 Mol. Chem. Phys.*, 1978, 74, 1607–1626.

5 G. V. Lowry, R. J. Hill, S. Harper, A. F. Rawle, C. O. Hendren, F. Klaessig, U. Nobbmann, P. Sayre and J. Rumble, *Environ. Sci. Nano*, 2016, **3**, 953–965.

6 C. P. Schulthess and D. L. Sparks, *Am. J. Soil Sci.* , 1986, **50**, 1406–1411.

7 M. Kosmulski and E. Mączka, *Colloids Surfaces A Physicochem. Eng. Asp.*, 2019, **575**, 140–143.

8 M. Kosmulski, *Surface Charging and Points of Zero Charge*, CRC Press, 2009.

9 J. A. Menendez-Diaz and I. Martín-Gullon, in *Activated Carbon Surfaces in Environmental Remediation*, ed. T. J. Bandosz, Elsevier Ltd, Oxford, 2006, pp. 1–45.

10 J. S. Mattson and H. B. J. Mark, *Activated carbon: Surface chemistry and adsorption from solution*, Marcel Dekker Inc., New York, 1971.

11 Malvern Instruments, *A basic guide to particle characterization*, 2015.

12 Anton Paar GmbH, The principles of dynamic light scattering, https://wiki.anton-paar.com/ca-en/the-principles-of-dynamic-light-scattering/, (accessed 18 April 2023).

13 Z. Shao, S. Luo, M. Liang, Z. Ning, W. Sun, Y. Zhu, J. Mo, Y. Li, W. Huang and C. Chen, *Water Res.*, 2021, **203**, 117561.

14 R. B. Baird, A. D. Eaton and E. W. Rice, Eds., *Standard methods For the examination of water and waste water*, American Public Health Association(APHA) American Water Works Association(AWWA) Water Environment Federation(WEF), Washington, DC, 23rd edn., 2017.

15 W. Kunz, *Curr. Opin. Colloid Interface Sci.*, 2010, **15**, 34–39.

16 N. Schwierz, D. Horinek, U. Sivan and R. R. Netz, *Curr. Opin. Colloid Interface Sci.*, 2016, **23**, 10–18.

17 H. I. Okur, J. Hladílková, K. B. Rembert, Y. Cho, J. Heyda, J. Dzubiella, P. S. Cremer and P. Jungwirth, *J. Phys. Chem. B*, 2017, **121**, 1997–2014.

18 T. Oncsik, G. Trefalt, M. Borkovec and I. Szilagyi, *Langmuir*, 2015, **31**, 3799–3807.

19 T. Oncsik, A. Desert, G. Trefalt, M. Borkovec and I. Szilagyi, *Phys. Chem. Chem. Phys.*, 2016, **18**, 7511–7520.

20 K. P. Gregory, G. R. Elliott, H. Robertson, A. Kumar, E. J. Wanless, G. B. Webber, V. S. J. Craig, G. G. Andersson and A. J. Page, *Phys. Chem. Chem. Phys.*, 2022, **24**, 12682–12718.

21 M. G. Cacace, E. M. Landau and J. J. Ramsden, *Q. Rev. Biophys.*, 1997, **30**, 241–277.

22 D. F. Parsons, M. Boström, P. L. Nostro and B. W. Ninham, *Phys. Chem. Chem. Phys.*, 2011, **13**, 12352–12367.

23 J. Kherb, S. C. Flores and P. S. Cremer, *J. Phys. Chem. B*, 2012, **116**, 7389–7397.

24 T. López-León, M. J. Santander-Ortega, J. L. Ortega-Vinuesa and D. Bastos-González, *J. Phys. Chem. C*, 2008, **112**, 16060–16069.

25 D. H. Napper, *J. Colloid Interface Sci.*, 1970, **33**, 384–392.

26 H. Wang, X. Zhao, X. Han, Z. Tang, S. Liu, W. Guo, C. Deng, Q. Guo, H. Wang, F. Wu, X. Meng and J. P. Giesy, *Sci. Total Environ.*, 2017, **586**, 817–826.

27 T. Rios-Carvajal, N. R. Pedersen, N. Bovet, S. L. S. Stipp and T. Hassenkam, *Langmuir*, 2018, **34**, 10254–10261.